ORIGINAL RESEARCH

Differentiation of Glioblastoma Multiforme and Single Brain Metastasis by Peak Height and Percentage of Signal Intensity Recovery Derived from Dynamic Susceptibility-Weighted Contrast-Enhanced Perfusion MR Imaging

S. Cha
J.M. Lupo
M.-H. Chen
K.R. Lamborn
M.W. McDermott
M.S. Berger
S.J. Nelson
W.P. Dillon

BACKGROUND AND PURPOSE: Glioblastoma multiforme (GBM) and single brain metastasis (MET) are the 2 most common malignant brain tumors that can appear similar on anatomic imaging but require vastly different treatment strategy. The purpose of our study was to determine whether the peak height and the percentage of signal intensity recovery derived from dynamic susceptibility-weighted contrast-enhanced (DSC) perfusion MR imaging could differentiate GBM and MET.

MATERIALS AND METHODS: Forty-three patients with histopathologic diagnosis of GBM ($n = 27$) or MET ($n = 16$) underwent DSC perfusion MR imaging in addition to anatomic MR imaging before surgery. Regions of interest were drawn around the nonenhancing peritumoral T2 lesion (PTL) and the contrast-enhancing lesion (CEL). T2* signal intensity-time curves acquired during the first pass of gadolinium contrast material were converted to the changes in relaxation rate to yield T2* relaxivity ($\Delta R2^*$) curve. The peak height of maximal signal intensity drop and the percentage of signal intensity recovery at the end of first pass were measured for each voxel in the PTL and CEL regions of the tumor.

RESULTS: The average peak height for the PTL was significantly higher ($P = .04$) in GBM than in MET. The average percentage of signal intensity recovery was significantly reduced in PTL (78.4% versus 82.8%; $P = .02$) and in CEL (62.5% versus 80.9%, $P < .01$) regions of MET compared with those regions in the GBM group.

CONCLUSIONS: The findings of our study show that the peak height and the percentage of signal intensity recovery derived from the $\Delta R2^*$ curve of DSC perfusion MR imaging can differentiate GBM and MET.

Glioblastoma multiforme (GBM) and single brain metastasis often pose a diagnostic dilemma on anatomic MR imaging and may require a surgical biopsy for a definitive diagnosis.[1,2] A history of systemic cancer and multiplicity of lesions are 2 of the most helpful criteria in differentiating metastatic brain tumor from GBM in a patient with a contrast-enhancing brain mass. However, the ability to differentiate GBM from single brain metastasis on anatomic MR imaging alone remains challenging because of their similar imaging appearance; in addition, a brain mass may be the first manifestation of disease in ≤30% of patients with systemic cancer.[3] It is clinically important to distinguish GBM from a single brain metastasis, because medical staging, surgical planning, and therapeutic decisions are vastly different for each tumor type.[4,5] Patients with GBM usually do not require systemic work-up, because tumor spread outside of the central nervous system is exceedingly rare. However, patients with suspected single metastasis may benefit from triple-dose contrast-enhanced MR imaging to detect any additional lesions.[6] Furthermore, any patient with suspected brain metastasis without a previous history of systemic cancer should undergo comprehensive systemic staging to determine the site of the primary carcinoma and evidence of distant metastasis before any surgical intervention or medical therapy.

Despite their similar anatomic MR imaging appearance, the ultrastructure of tumor capillaries is markedly different between GBM and a brain metastasis. The GBM capillaries have various degrees of blood-brain barrier (BBB) disruption and a variety of morphologic features, including glomeruloid capillaries, simple vascular hyperplasia, and delicate neocapillaries, which simulate normal brain vessels.[7] As a result of this heterogeneous capillary morphology, the degree of permeability across GBM capillaries can vary from relatively normal to increased. The capillaries of brain metastasis, on the other hand, resemble those from the site of the original systemic cancer and thus have no similarity to the normal brain capillaries and completely lack BBB components with prominent capillary fenestration.[8] This unique capillary morphology results in greatly increased capillary permeability uniformly throughout the tumor vasculature,[9] causing vasogenic edema, which is readily detectable on MR imaging as a nonenhancing T2 abnormality surrounding the contrast-enhancing tumor.

To capture the morphologic and functional status of tumor capillaries on imaging, dynamic susceptibility-weighted contrast-enhanced (DSC) perfusion MR imaging, which exploits contrast agent behavior within the intravascular compartment

Received April 21, 2006; accepted after revision November 1.

From the Department of Radiology (S.C., J.M.L., M.-H.C., S.J.N., W.P.D.), Neuroradiology Section and the Department of Neurological Surgery (S.C., K.R.L., M.W.M., M.S.B., W.P.D.), University of California, San Francisco Medical Center, San Francisco, Calif

This work was supported by National Institutes of Health Grants NS045013 and P50-CA97297, and Accelerate Brain Cancer Cure.

Address correspondence to Soonmee Cha, MD, Department of Radiology, University of California, San Francisco, UCSF Medical Center, 505 Parnassus Ave, Box 0628, Room L358, San Francisco, CA 94143-0628; e-mail: soonmee.cha@radiology.ucsf.edu

DOI 10.3174/ajnr.A0484

of the brain, has been widely used in the clinical setting.[10-12] The relative cerebral blood volume (rCBV), the most robust and standard hemodynamic variable derived from DSC perfusion MR imaging, has been shown to correlate with astrocytoma grade[10,11,13] and histopathologic quantification of vascular hyperplasia.[10] However, there are 2 major shortcomings associated with rCBV measurement in malignant brain tumors. First, the calculation of tumor rCBV in contrast-enhancing tumors, such as GBM and brain metastasis, is complicated by disruption or lack of a BBB within the tumor capillaries, necessitating a correction for the underestimation or overestimation of rCBV as a result of contrast agent leakage during the first pass.[14] Second, tumor rCBV measurements, which reflect gross tumor blood volume, do not provide any information on capillary permeability. There have been a number of publications investigating the measurement of vascular permeability of tumor vasculature, which have demonstrated its use in predicting tumor biology.[15-18] A recent published report introduced 2 hemodynamic variables derived from DSC perfusion MR imaging (the peak height and the percentage of signal intensity recovery[19]) that may provide additional information on tumor vasculature. The peak height, defined as the maximal signal intensity drop from the precontrast baseline during the bolus phase of the first pass of gadolinium, has been shown to correlate with rCBV[20] and thus to reflect total capillary volume. On the other hand, the percentage of signal intensity recovery, defined as the percentage of signal intensity recovery relative to the precontrast baseline at the end of the first pass, is influenced by the amount of contrast agent leakage during the first pass and thus reflects alteration in capillary permeability.

The hypothesis of this study is that the peak height of the nonenhancing T2 region and the percentage of signal intensity recovery of the contrast-enhancing region in GBM are significantly higher than those of single brain metastasis, thus allowing preoperative differentiation between the 2 types of tumors. The purpose of our study was to use the 2 hemodynamic variables, peak height and percentage of signal intensity recovery, obtained from the analysis of the $T2^*$ relaxivity curve from DSC perfusion MR imaging, in assessing tumor capillary volume and permeability in regions of T2 abnormality and contrast enhancement of the tumor to distinguish between GBM and single brain metastasis.

Materials and Methods

Patients and Histopathologic Diagnosis

We recruited 43 patients who were presumed to have a solitary high-grade glioma based on initial contrast-enhanced MR imaging and who were referred to our institution for surgery from June 2002 to June 2004. Patients with multiple brain lesions, nonenhancing tumor, or clinical history of any therapy to the brain were excluded.

Five of the 43 patients had a remote history of breast carcinoma 3–8 years before presentation of brain tumor. In these 5 patients, primary high-grade glioma was still suspected, because all had a single large brain mass and no evidence of systemic cancer recurrence. All of the patients underwent gross total or near total resection of the contrast-enhancing tumor for a presumptive diagnosis of high-grade glioma. Informed consent was obtained from all of the patients under a protocol approved by our institutional review board.

Histopathologic analysis of the resected tissue confirmed the diagnosis of GBM in 27 patients and brain metastasis (9 breast carcinoma and 7 lung carcinoma) in 16 patients. Patients with GBM consisted of 17 men and 10 women (age range, 21–65 years; mean age, 51.7 years). There were 2 patients with giant cell histologic subtype GBM. The single brain metastasis cohort consisted of 4 men and 12 women (age range, 46–72 years; mean age, 59.2 years). Five women of the 16 patients with a brain metastasis had a known history of systemic malignancy, all with remote history of breast carcinoma.

MR Imaging

All of the patients underwent the same preoperative MR imaging protocol by using a 1.5T MR scanner (GE Medical Systems, Milwaukee, Wis). The protocol consisted of the following sequences: 3-plane localizer (8.5 ms/1.6 ms, TR/TE), transverse fluid-attenuated inversion recovery (FLAIR; 10,000 ms/148 ms/2200 ms, TR/TE/TI), transverse fast spin-echo (FSE) T2-weighted (3000 ms/102 ms, TR/TE), DSC gradient-echo echo-planar (1000–1250 ms/54 ms, TR/TE; flip angle, 35°), and contrast-enhanced 3D spoiled gradient-recalled acquisition in the steady state (SPGR) T1-weighted (34 ms/8 ms, TR/TE) imaging. For DSC gradient-echo echo-planar imaging, the location and size of the tumor and the position of the superior and inferior margins were determined from the FLAIR and fast spin-echo images. Seven to 8 sections (3–5 mm thick, gap of 0–1 mm) were selected to cover the entire tumor volume. A standard dose of contrast agent, gadopentetate dimeglumine (Gd-DTPA; 0.1 mmol/kg body weight; Omniscan, GE Medical Systems) was injected intravenously with an MR-compatible power injector (Medrad, Indianola, Pa) at a rate of 4 or 5 mL/s through an antecubital angiocatheter (18–21 gauge), followed immediately by a 20-mL continuous saline flush. The multisection image set was acquired every 1.25 s during the first pass of the contrast agent Gd-DTPA until 60 time points were obtained.

The TE and flip angle for DSC MR imaging were chosen based on our past experience with optimizing the perfusion sequence. A TE of 54 ms was chosen for the gradient-echo technique to maximize the effect of susceptibility changes, whereas a flip angle of 35° was selected to minimize T1 effect during the first pass. Altering TE or flip angle would most likely alter the time intensity curve characteristic during the first pass. By increasing TE and flip angle, we would expect the maximal peak height to decrease and percentage of signal intensity recovery to increase, respectively.

Image Processing

The FLAIR, fast spin-echo, contrast-enhanced 3D SPGR, and raw DSC gradient-echo echo-planar images were transferred to a UNIX workstation (Sun Microsystems, Mountain View, Calif) for off-line postprocessing. Image processing was performed using custom software written in C and IDL programming languages (Research Systems, Boulder, Colo). The FLAIR, FSE, and contrast-enhanced 3D SPGR images were resampled to the same section locations and resolution as that of the echo-planar perfusion images. The dynamic dataset was aligned to the anatomic images using affine and perspective transformations and, where necessary, nonrigid B-spline warping[21] by maximization of normalized mutual information.[22] The nonrigid registration techniques were performed to ensure accurate alignment between the perfusion dataset and the anatomic regions defined by the T1- and T2-weighted images. The registration was performed with the use of the VTK CISG Registration Toolkit (open source code from King's College, London, UK) by optimizing the positions of a 3D lattice of cubic B-spline control points. Initially, the control points

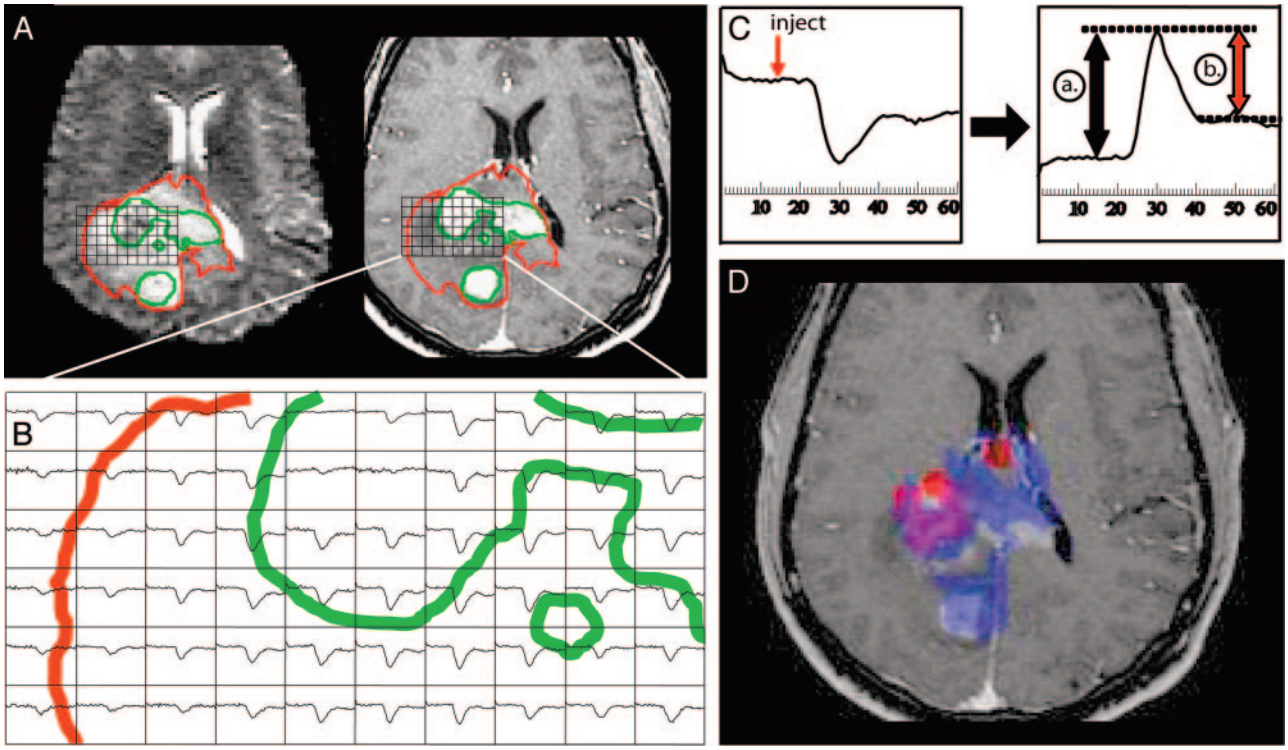

Fig 1. A 46-year-old man with right parietal and corpus callosal GBM. Transverse T2* susceptibility echo-planar perfusion image (*left*) and contrast-enhanced SPGR T1-weighted image (*right*) (*A*) and corresponding T2* susceptibility signal intensity time curves of T2 lesion (*red*) and contrast-enhancing lesion (*green*) (*B*) demonstrate variation in signal intensity characteristics in the tumor. T2* susceptibility signal intensity time curve (*C, left*) is converted to ΔR2* curve (*right*) by using the following formula: $\Delta R2^* = -\ln(S_t/S_0)/TE$, where ln is natural log and S_t and S_0 are signal intensities at time *t* and 0. In the ΔR2* curve (*right*), the peak height is represented as *a*, and the percentage of signal intensity recovery is the percentile of *b*/*a*. Transverse contrast-enhanced SPGR T1-weighted image (*D*) is overlaid with areas of abnormal peak height (*blue*) and percentage of signal intensity recovery less than 50% (*red*) and shows a large area of increased vascularity (*blue*) with a peripheral region of high permeability (*red*) in this GBM.

are regularly spaced and then optimized through a steepest-ascent search algorithm that maximized a normalized mutual information cost function. A finer initial control point spacing (5 mm compared with 10 mm) was selected for the phase-encode direction when there were larger displacements. These nonrigid registration techniques are computationally intensive and would be relevant in the clinical setting only if the location of the lesion was in a region with high geometric distortion (ie, above the sinuses). Most lesions that are more centrally located would not need to undergo this form of registration unless the goal is to use the perfusion parameters in conjunction with other anatomic or functional images to delineate tumor boundaries for treatment planning or surgery.

The aligned perfusion series was then resampled to a 32 × 32 voxel grid in-plane with a 16 × 16-cm^2 FOV so that the observed signal intensity changes had sufficient signal-to-noise ratio to be analyzed reliably on a voxel-by-voxel basis. DSC MR imaging was performed only in the axial plane. However, the DSC dataset was aligned to the 3D postcontrast SPGR image set to yield perfusion color maps that were interpolated in all 3 of the planes. The pixel size was increased to a 5 × 5-mm^2 resolution to ensure that errors in the alignment to anatomic images due to geometric distortion would be contained within 1 voxel. This oversampling was comparable with most other studies that draw several regions of interest (ROIs), each encompassing approximately 20 2 × 2-mm^2 voxels, to obtain several hemodynamic measurements in the same region from which to calculate a maximum value.

For each tumor, ROIs were drawn around the entire contrast-enhancing portion of the lesion and the peritumoral T2 lesion (ie, T2 abnormality outside of contrast-enhancing lesion and central area of necrosis) from the resampled contrast-enhanced 3D SPGR (Fig 1) and either FLAIR or FSE images, respectively. Regions of signal intensity drop-out caused by susceptibility on the echo-planar images and areas of nonenhancing necrotic regions of the tumor were excluded from the ROIs, because the T2* signal intensity time curves within these voxels did not pass a certain signal-to-noise threshold to reliably quantify. A neuroradiologist (S.C.) approved all of the ROIs. The resampled echo-planar image for a single section of the first image set and corresponding T2* susceptibility signal intensity–time curves are displayed in Fig 1*A*, -*B*, with overlaying contours depicting the extent of the T2 lesion (in *red*) and contrast-enhancing region (in *green*).

T2 Signal Intensity-Time Curve Analysis From DSC Perfusion MR Imaging*

Figure 2 demonstrates an example of various T2* susceptibility signal intensity-time curve characteristics in normal gray and white matter, as well as in a brain metastasis. The resampled T2* signal intensity time curves acquired during the first pass of gadolinium bolus were converted to the change in relaxation rate (ΔR2*). The precontrast baseline signal intensity, S_0, was established from 6 image volumes acquired before contrast injection. Because the relative Gd-DTPA concentration is proportional to the ΔR2* curve, a plot of the relative concentration of Gd-DTPA in tissue over time was obtained for each voxel. Peak height and percentage of recovery of the postbolus signal intensity from the peak were calculated from the ΔR2* curve of the perfusion data for each voxel within the defined ROI. Peak height values were normalized to the peak of a model curve function derived from a normal-appearing brain based on histogram analysis of the precontrast echo-planar images.[19] Voxels with peak height values

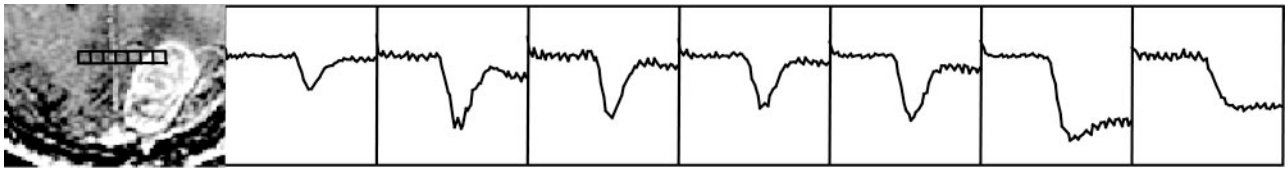

Fig 2. Left occipital single breast cancer metastasis in a 62-year-old woman. Transverse contrast-enhanced SPGR T1-weighted image (*left*) and a strip of T2* susceptibility signal intensity time curve through normal brain and left occipital metastatic brain tumor demonstrate increased peak height and marked loss in signal intensity recovery in the tumor (*2 voxels on right*) consistent with vascular and permeable metastatic tumor vasculature.

Table 1: Volumes of abnormality expressed as a percentage of the entire T2 lesion for GBM and single brain metastasis

Tumor	Contrast-Enhancing Lesion	Necrosis	Abnormal Peak Height	<50% SI Recovery/ T2 L	>75% SI Recovery/ T2 L
GBM (n = 27)	28.8 (31.5)	14.8 (18.6)	22.2 (22.7)	0.4 (1.1)	79.5 (16.7)
MET (n = 16)	24.3 (28.0)	12.0 (17.3)	9.2 (19.1)	8.6 (25.6)	52.2 (42.6)
Wilcoxon P value	>.5	.44	.14	<.01	<.01

Note:—GBM indicates glioblastoma multiforme; MET, single brain metastasis; SI, signal intensity; T2 L, entire T2 lesion. Data are median percentages. Numbers in parentheses are interquartile range.

more than twice the model curve were classified as having abnormal peak height, whereas those in which the postbolus concentration recovered by less than 75% from the peak concentration were considered to have abnormal recovery.

Volumes of abnormal peak height, no signal intensity loss (necrosis), contrast enhancement, less than 50% signal intensity recovery, and more than 75% signal intensity recovery were calculated and normalized according to the T2 lesion volume on the perfusion images. Median, average, and maximum peak height values, as well as median, average, and minimum percentage of signal intensity recovery, were calculated in the contrast-enhancing lesion region, the entire T2 lesion, and the T2 lesion excluding contrast enhancement and necrosis (peritumoral lesion region). We chose median values because they were less affected by the extreme values and, therefore, were more robust than means in terms of describing the central tendency of the distribution. Nonparametric methods were applied throughout the article when more appropriate than parametric methods.

Statistical Analysis

For initial univariate analysis, the Wilcoxon rank sum test was used to compare GBM and single brain metastasis. A $P < .05$ was considered to indicate a statistically significant difference. The ultimate goal was to identify a model that could be used clinically to predict preoperatively whether a patient has a GBM or a single brain metastasis. The number of lesions in our study was small relative to the number of variables considered. However, to provide preliminary information, a multivariate logistic regression with a stepwise variable selection procedure was carried out to identify the subset of variables that is most predictive of tumor type. The method of classification and regression tree analysis (referred to as classification and regression tree analysis and also as recursive partitioning analysis) was used to determine whether this method identified the same variables and provided a similar assessment of a clinically applicable decision rule for separating patients with GBM from those with single brain metastasis on the basis of perfusion MR imaging variables.

Results

Tumor Volumes with Abnormal Peak Height and Percentage of Signal Intensity Recovery

The volumes of abnormal peak height (ie, peak height more than twice the normal brain model function) and less than 50% signal intensity recovery were expressed as a ratio to the volume of the entire T2 lesion (Table 1). Considerable heterogeneity was noted in both the shape of the dynamic concentration curves and in the volume of less than 50% recovery in the GBM and single brain metastasis groups (Fig 3). As expected, the contrast-enhancing tumor volumes were similar between both groups (medians, 28.8% versus 24.3%, GBM versus metastasis). There was a tendency for the volume of abnormal peak height in the GBM group to be larger than that in the metastasis group (medians, 22.2% versus 9.2%), but this difference was not statistically significant. Volumes of less than 50% signal intensity recovery were significantly larger for the metastasis group than for the GBM group (medians, 8.6% versus 0.4%; $P < .01$). Volumes of more than 75% signal intensity recovery representing close-to-normal recovery pat-

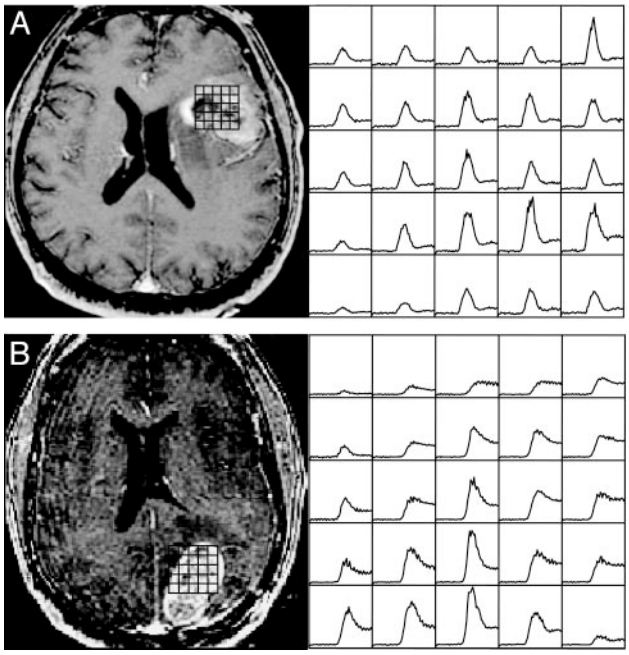

Fig 3. Axial contrast-enhanced SPGR T1-weighted images (*left*) and T2* relaxivity signal intensity time curves (*right*) in GBM (*A*) and breast cancer metastasis (*B*) show a marked difference in percentage of signal intensity recovery at the end of the first pass where GBM has far more than 50% signal intensity recovery to the baseline compared with the metastasis.

Table 2: Relative peak height and percentage of signal recovery in contrast-enhancing lesion regions

Tumor	Maximum Peak Height	Average Peak Height	Minimum Percentage of Signal Recovery	Average Percentage of Signal Recovery
GBM ($n = 27$)	4.6 (3.6)	1.8 (0.9)	50.2 (21.6)	80.9 (9.1)
Metastasis ($n = 16$)	5.0 (3.7)	1.6 (0.9)	25.4 (34.8)	62.5 (16.4)
Wilcoxon *P* value	.52	.25	<.01	<.01

Note:—Data are median values. Unit of measure for peak height is in arbitrary unit. Numbers in parentheses are interquartile range.

Table 3: Relative peak height and percentage of signal recovery in peritumoral nonenhancing lesion region

Tumor	Maximum Peak Height	Average Peak Height	Minimum Percentage of Signal Recovery	Average Percentage of Signal Recovery
GBM ($n = 27$)	5.5 (3.1)	1.1 (0.8)	46.8 (26.6)	82.8 (3.9)
Metastasis ($n = 16$)	3.9 (2.4)	0.9 (0.3)	33.1 (21.5)	78.4 (12.8)
Wilcoxon *P* value	.13	.04	.02	.02

Note:—Data are median values. Numbers in parentheses are interquartile range.

terns as determined by a previous study[19] were significantly greater for the GBM group than the metastasis group (medians, 79.5% versus 52.2%; $P < .01$).

Peak Height

In the contrast-enhancing regions, the GBM and metastasis groups exhibited similar average (medians, 1.8 and 1.6) and maximum (medians, 4.6 and 5.0) relative peak height values (Table 2). In the peritumoral lesion region (Table 3), patients with GBM had slightly higher average (medians, 1.1 and 0.9) and maximum (medians, 5.5 and 3.9) peak height values compared with those values in the patients with metastasis, but this difference was only statistically significant for the average peak height values ($P = .04$). Thus, the average peak height was significantly higher in the contrast-enhancing regions than in the surrounding peritumoral lesion region in both tumor types ($P < .01$). It is noteworthy that the 2 cases of giant cell GBM had the 2 lowest peak height values in the peritumoral region compared with the more common infiltrative GBMs.

Percentage of Signal Intensity Recovery

The percentage of signal intensity recovery of the model function of a normal portion of the brain in the GBM and metastasis groups did not differ significantly, because none of the patients had additional lesions other than the dominant mass, and no patients received previous treatment. Unlike the peak height measurements, the differences in the average and minimum percentage of signal intensity recovery between the 2 groups of tumors were highly significant in all of the regions (contrast-enhancing lesion, T2 lesion, and peritumoral lesion), as noted in Tables 2–4. Both the minimum and average percentages of signal intensity recovery were significantly greater in all of the regions for patients with GBM compared with the values for patients with metastasis ($P < .05$). Figure 4 demonstrates color overlay maps of abnormal peak height and percentage of signal intensity recovery maps in a GBM and a breast cancer metastasis.

Probability Model Based on Statistical Analysis

The average percentage of signal intensity recovery in the contrast-enhancing lesion and in the peritumoral T2 lesion most effectively divided GBM from single brain metastasis. Multivariate logistic regression with stepwise selection and a cutoff *P* value of .05 selected average percentage of signal intensity recovery values in the contrast-enhancing lesion region alone as most effective in dividing the 2 groups. No patient with GBM had an average percentage of signal intensity recovery in the contrast-enhancing region of less than 66%, and 11 of 16 patients with a metastasis had values below this cutoff point. No patient with metastasis had an average percentage of signal intensity recovery in the contrast-enhancing lesion region of more than 84%, and 10 of 27 patients with GBM had values above this cutoff point. The recursive partitioning analysis also selected average percentage of signal intensity recovery in the contrast-enhancing region as the most predictive of tumor type. From the logistic regression analysis, the estimated probability of predicting that a tumor is not a GBM and observing the actual GBM were plotted (Fig 5), which showed that the average percentage of signal intensity recovery of ≤66% within the contrast-enhancing region of the tumor had a specificity of 100% and a sensitivity of 69% in correctly identifying that a tumor is not a GBM.

Discussion

In this study, we used 2 hemodynamic variables (peak height and percentage of signal intensity recovery) derived from the $\Delta R2^*$ curve of DSC perfusion MR imaging to differentiate GBM and single brain metastasis, both of which can appear similar on conventional anatomic MR images. We found that the average peak height in the nonenhancing peritumoral T2 region (PTL) is significantly higher in GBM than in single brain metastasis. Similarly, the average percentage of signal intensity recovery in the contrast-enhancing region is significantly higher in GBM than in single brain metastasis.

The increases in peak height observed in the PTL region of GBMs are supported by the elevated rCBV found in the PTL region of GBMs by Law et al.[23] As suggested by the report, the difference in rCBV, or the peak height in our study, in the PTL region of GBM and single brain metastasis is due to distinct pathophysiologic changes in vasculature between the 2 tumor types. Kelly et al[24] have shown that the PTL region of GBM on MR imaging corresponds with a heterogeneous mixture of vasogenic edema, infiltrating glioma cells, and neoplastic capillaries on histopathology. On the other hand, the PTL region of brain metastasis represents pure vasogenic edema resulting from uncontrolled leakage of blood plasma into the interstitial compartment because of leaky capillaries.[8,25] Similar to the rCBV measurements in PTL region, our study also found that

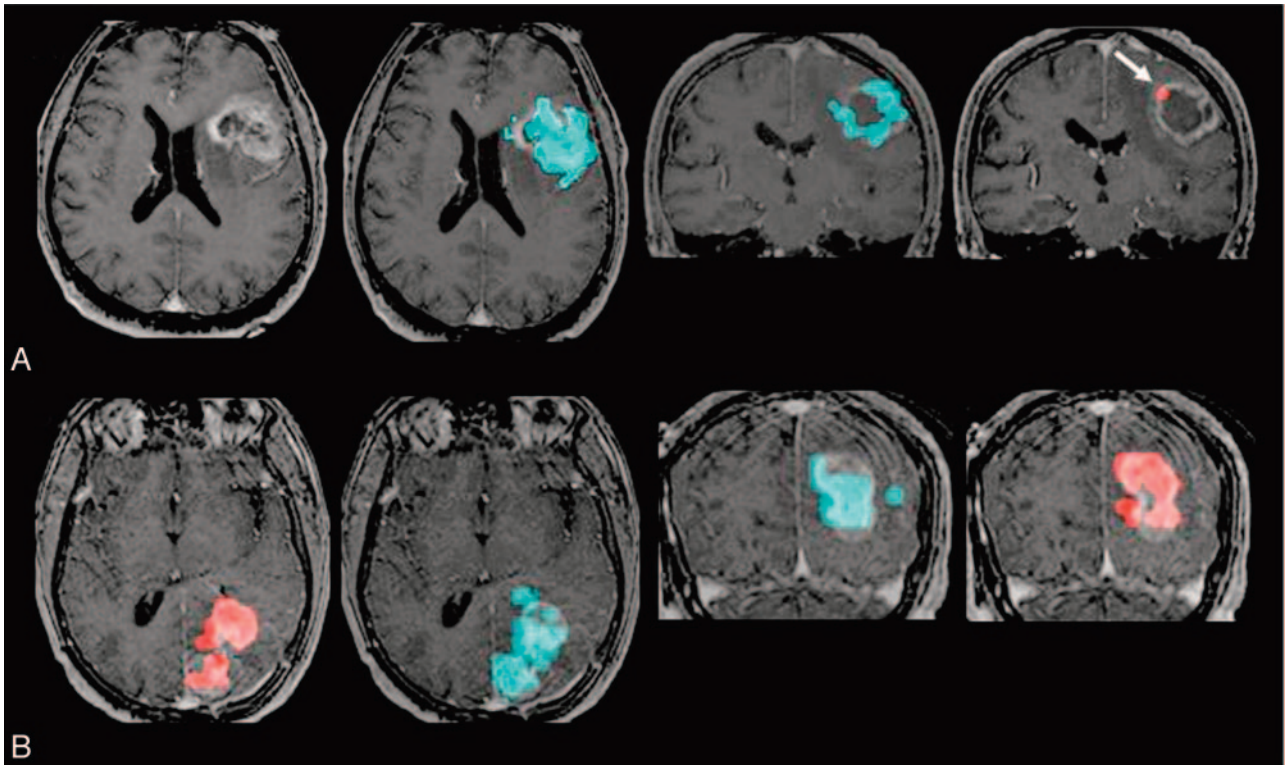

Fig 4. Abnormal peak height and percentage of signal intensity recovery maps in a GBM (*A*) and a breast cancer metastasis (*B*). The *blue overlay* represents an area of abnormal peak height (greater than twice the normal brain) and *pink overlay* depicts area of less than 50% signal intensity recovery of T2* relaxivity curve.

A, Top row, left frontal GBM in a 45-year-old man. Axial (*2 left images*) and coronal (*2 right images*) contrast-enhanced T1-weighted images show a large area of peak height abnormality (*blue*) but only a small area of less than 50% signal intensity recovery (*arrow, pink*), suggesting highly vascular but not permeable vessels.

B, Bottom row, left occipital breast cancer metastasis in a 62-year-old woman. Axial (*2 left images*) and coronal (*2 right images*) contrast-enhanced T1-weighted images demonstrate large areas of both abnormal peak height (*blue*) and less than 50% signal intensity recovery (*pink*), suggesting vascular but also highly permeable microvasculature of the metastatic tumor.

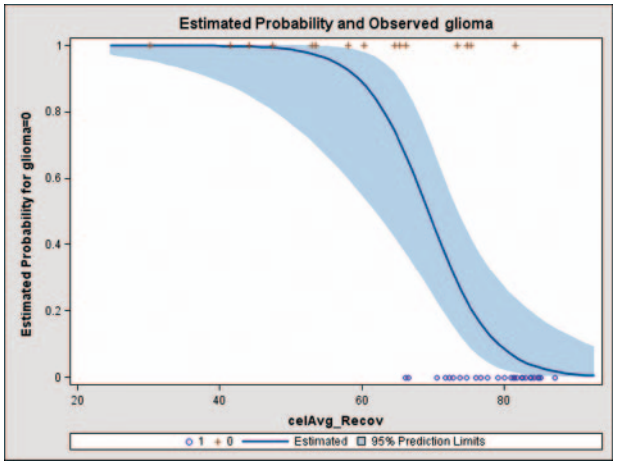

Fig 5. Estimated probability and observed glioma (GBM) curve based on logistic regression analysis. Y-axis represents the estimated probability that a tumor is not a GBM, and the x-axis represents the average percentage of signal intensity recovery (celAvg_Recov) within the contrast-enhancing lesion of the tumor. This curve shows that when a cutoff of ≤66% signal intensity recovery is used, there is 100% specificity to correctly predict that a tumor is not a GBM with a sensitivity of 69%. The *small circle* (○) represents GBM, and the *plus sign* (+) represents metastasis. The *shaded area* is the confidence interval.

the peak height, which has been shown to correlate strongly with rCBV,[20] is significantly higher in the PTL region of GBM, probably because of higher capillary attenuation.

The significant difference in the percentage of signal intensity recovery between GBM and brain metastasis is probably due to the profound difference in capillary permeability between the 2 tumor types shown by several histologic studies on tumor capillary morphology. Rojiani and Dorovini-Zis[26] showed that GBM microvasculature is composed of closely packed, newly formed capillary buds, lined by hyperplastic endothelial cells that are partly invested by pericytes and can retain some aspects of BBB architecture. In 1979, Long[9] eloquently described the capillary ultrastructure in 18 metastatic brain tumors by using electron microscopy. His results showed that capillaries of metastatic brain tumor resemble those of systemic origin instead of those present in healthy brain tissue. As a result, capillaries of metastatic brain tumor are highly permeable to protein-bound radiotracers because of a defective endothelium and are completely devoid of any rudimentary BBB architecture unique to normal brain capillaries. Our findings suggest that the capillary permeability within the contrast-enhancing region of GBM and single brain metastasis is markedly different; the capillaries of brain metastasis, which resemble the capillaries of primary systemic cancer, are much leakier because of complete absence of BBB.

Multivariate logistic regression analysis allowed us to identify the average percentage of signal intensity recovery in the contrast-enhancing lesion as the most powerful predictor to correctly predict each tumor type. Based on this predictive statistical modeling, we found that, when the average percentage of signal intensity recovery in the contrast-enhancing lesion is more than 82% and less than 66%, the prediction of GBM and single brain metastasis, respectively, had specificity of 100%.

The volume results of our study showed that the contrast-

enhancing tumor volume and nonenhancing necrosis volume were similar in GBM and single brain metastasis as expected, because both are avidly enhancing masses with significant BBB destruction and necrosis. An increasing trend persisted in the volume of abnormal peak height (which included both enhancing and nonenhancing components) from single brain metastasis to GBM. The volume of abnormal peak height most likely reflects the intensity and extent of tumor angiogenesis. Therefore, it is not surprising to find that GBM had a higher value than that of single brain metastasis, because GBM tends to have angiogenesis beyond the contrast-enhancing portion of the tumor, whereas, in single brain metastasis, the nonenhancing T2 abnormality represents vasogenic edema without tumor. The volume of tumor showing less than 50% signal intensity recovery during the recirculation phase was much greater in single brain metastasis than in GBM, most likely reflecting the greater degree of alteration of capillary permeability in the single brain metastasis group. A greater volume of tissue with less than 50% recovery is expected in single brain metastasis, because the capillaries of these tumors are highly permeable as a result of their complete lack of BBB.

In this study, we chose 2 variables, peak height and percentage of signal intensity recovery, to describe the shape of the dynamic perfusion data. This choice was dictated by our desire to minimize the dependence on complex, nonlinear fitting procedures as would be required in blood volume calculation for tumors with altered or absent BBB and to provide robust estimates of meaningful hemodynamic parameters that can be obtained with relative ease and used in clinical interpretation of images. The calculations of peak height and percentage of signal intensity recovery were simple to implement and were relatively insensitive to signal-to-noise ratio changes. Although there was some variation in observed peak widths, the time to peak was remarkably similar (within 1-s time point) for both the normal and tumor voxels within a given individual patient. This suggested that there was a close correspondence between the T2* signal intensity changes due to bolus passage of Gd-DTPA and the underlying rCBV as reported previously.[20] On a practical note, the peak height and percentage of signal intensity recovery can be easily quantified on a vendor-supplied workstation, without sophisticated off-line software packages, and, hence, become part of a diagnostic armamentarium to improve the diagnosis and understanding of brain diseases, especially brain tumors.

In conclusion, although the relatively small sample of this study cautions against overinterpretation, our results suggest that quantitative analysis of T2* relaxivity signal intensity–time curve characteristics from DSC MR imaging provides information on tumor vascular properties that adds specificity to differentiating GBM and single brain metastasis, which often share similar conventional anatomic MR imaging findings. Based on the significant difference in the peak height and percentage of signal intensity recovery obtained from the T2* signal intensity time curve between GBM and single brain metastasis, we conclude that DSC perfusion MR imaging substantially improves the prediction of tumor type before surgery. This added information will lead not only to a better understanding of how tumor vasculature affects imaging but also to improved preoperative management and intraoperative strategies in patients with a contrast-enhancing brain tumor.

References

1. Davis FG, McCarthy BJ, Berger MS. **Centralized databases available for describing primary brain tumor incidence, survival, and treatment: Central Brain Tumor Registry of the United States; Surveillance, Epidemiology, and End Results; and National Cancer Data Base.** *Neuro-oncol* 1999;1:205–11
2. Surawicz TS, McCarthy BJ, Kupelian V, et al. **Descriptive epidemiology of primary brain and CNS tumors: results from the Central Brain Tumor Registry of the United States, 1990–1994.** *Neuro-oncol* 1999;1:14–25
3. Schiff D. **Single brain metastasis.** *Curr Treat Options Neurol* 2001;3:89–99
4. Giese A, Westphal M. **Treatment of malignant glioma: a problem beyond the margins of resection.** *J Cancer Res Clin Oncol* 2001;127:217–25
5. O'Neill BP, Buckner JC, Coffey RJ, et al. **Brain metastatic lesions.** *Mayo Clin Proc* 1994;69:1062–68
6. Yuh WT, Tali ET, Nguyen HD, et al. **The effect of contrast dose, imaging time, and lesion size in the MR detection of intracerebral metastasis.** *AJNR Am J Neuroradiol* 1995;16:373–80
7. Wesseling P, Ruiter DJ, Burger PC. **Angiogenesis in brain tumors; pathobiological and clinical aspects.** *J Neurooncol* 1997;32:253–65
8. Jinnouchi T, Shibata S, Fukushima M, et al. **Ultrastructure of capillary permeability in human brain tumor–Part 6: Metastatic brain tumor with brain edema** [in Japanese]. *No Shinkei Geka* 1988;16:563–68
9. Long DM. **Capillary ultrastructure in human metastatic brain tumors.** *J Neurosurg* 1979;51:53–58
10. Aronen HJ, Gazit IE, Louis DN, et al. **Cerebral blood volume maps of gliomas: comparison with tumor grade and histologic findings.** *Radiology* 1994;191:41–51
11. Knopp EA, Cha S, Johnson G, et al. **Glial neoplasms: dynamic contrast-enhanced T2*-weighted MR imaging.** *Radiology* 1999;211:791–98
12. Sugahara T, Korogi Y, Kochi M, et al. **Correlation of MR imaging-determined cerebral blood volume maps with histologic and angiographic determination of vascularity of gliomas.** *AJR Am J Roentgenol* 1998;171:1479–86
13. Lev MH, Ozsunar Y, Henson JW, et al. **Glial tumor grading and outcome prediction using dynamic spin-echo MR susceptibility mapping compared with conventional contrast-enhanced MR: confounding effect of elevated rCBV of oligodendrogliomas.** *AJNR Am J Neuroradiol* 2004;25:214–21
14. Heiland S, Benner T, Debus J, et al. **Simultaneous assessment of cerebral hemodynamics and contrast agent uptake in lesions with disrupted blood-brain-barrier.** *Magn Reson Imaging* 1999;17:21–27
15. Law M, Yang S, Babb JS, et al. **Comparison of cerebral blood volume and vascular permeability from dynamic susceptibility contrast-enhanced perfusion MR imaging with glioma grade.** *AJNR Am J Neuroradiol* 2004;25:746–55
16. Li KL, Zhu XP, Checkley DR, et al. **Simultaneous mapping of blood volume and endothelial permeability surface area product in gliomas using iterative analysis of first-pass dynamic contrast enhanced MRI data.** *Br J Radiol* 2003;76:39–50
17. Provenzale JM, Wang GR, Brenner T, et al. **Comparison of permeability in high-grade and low-grade brain tumors using dynamic susceptibility contrast MR imaging.** *AJR Am J Roentgenol* 2002;178:711–16
18. Roberts HC, Roberts TP, Bollen AW, et al. **Correlation of microvascular permeability derived from dynamic contrast-enhanced MR imaging with histologic grade and tumor labeling index: a study in human brain tumors.** *Acad Radiol* 2001;8:384–91
19. Lupo JM, Cha S, Chang SM, et al. **Dynamic susceptibility-weighted perfusion imaging of high-grade gliomas: characterization of spatial heterogeneity.** *AJNR Am J Neuroradiol* 2005;26:1446–54
20. Cha S, Lu S, Johnson G, et al. **Dynamic susceptibility contrast MR imaging: correlation of signal intensity changes with cerebral blood volume measurements.** *J Magn Reson Imaging* 2000;11:114–19
21. Rueckert D, Frangi AF, Schnabel JA. **Automatic construction of 3-D statistical deformation models of the brain using nonrigid registration.** *IEEE Trans Med Imaging* 2003;22:1014–25
22. Studholme C, Novotny E, Zubal IG, et al. **Estimating tissue deformation between functional images induced by intracranial electrode implantation using anatomical MRI.** *Neuroimage* 2001;13:561–76
23. Law M, Cha S, Knopp EA, et al. **High-grade gliomas and solitary metastases: differentiation by using perfusion and proton spectroscopic MR imaging.** *Radiology* 2002;222:715–21
24. Kelly PJ, Daumas-Duport C, Scheithauer BE, et al. **Stereotactic histologic correlations of computed tomography and magnetic resonance imaging defined abnormalities in patients with glial neoplasms.** *Mayo Clin Proc* 1987;62:450–59
25. Strugar J, Rothbart D, Harrington W, et al. **Vascular permeability factor in brain metastases: correlation with vasogenic brain edema and tumor angiogenesis.** *J Neurosurg* 1994;81:560–66
26. Rojiani AM, Dorovini-Zis K. **Glomeruloid vascular structures in glioblastoma multiforme: an immunohistochemical and ultrastructural study.** *J Neurosurg* 1996;85:1078–84